gered pattern of $+N_f$ and $-N_f$ observed in Fig. 3b shows that the convection velocities of the dominant structures in the two half-planes of the excited coaxial jet are different. This phenomenon eventually results in the formation of the asymmetric structures in the fully merged zone of the jet.

Conclusions

Results of the present study provide pictures on the interactions between flow structures in the initial region of an excited coaxial jet of $\lambda^{-1}=0.3$. Two trains of vortical structures are recovered in the inner mixing layer of the jet. Also, there exist at least two different types of inner vortices interactions before the end of the inner potential core. They are the incomplete coalescence and the amalgamation process. These interactions, which are different from those observed in a single circular jet, eventually give rise to asymmetric flow structures beyond the initial merging zone. A new structure with outwardly rotating circulation appears in the intermediate merging zone. Interaction between the w vortex and coflowing wake vortex in the intermediate merging zone is more rigorous than that between the w vortex and the new vortex. The dominant structures in the positive and negative half-planes also convect at different velocities at the end of the intermediate merging zone.

Acknowledgments

This work was partly supported by grants from the Committee of Conference and Research Grants and the Leung Kau Kui Research and Teaching Endowment Fund, the University of Hong Kong.

References

[1]Champagne, F. H., and Wygnanski, I. J., "An Experimental Investigation of Coaxial Jet," *International Journal of Heat and Mass Transfer,* Vol. 14, 1971, pp. 1445–1461.

[2]Kwan, A. S. H., and Ko, N. W. M., "Coherent Structures in Subsonic Coaxial Jets," *Journal of Sound and Vibration,* Vol. 48, No. 1, 1976, pp. 203–219.

[3]Ko, N. W. M., and Au, H., "Coaxial Jets of Different Mean Velocity Ratios," *Journal of Sound and Vibration,* Vol. 100, No. 2, 1985, pp. 211–232.

[4]Au, H., and Ko, N. W. M., "Coaxial Jets of Different Mean Velocity Ratios, Pt. 2," *Journal of Sound and Vibration,* Vol. 116, No. 3, 1987, pp. 427–443.

[5]Ko, N. W. M., and Chan, W. T., "The Inner Region of Annular Jet," *Journal of Fluid Mechanics,* Vol. 93, Pt. 3, 1979, pp. 549–584.

[6]Perry, A. E., and Lim, T. T., "Coherent Structures in Coflowing Jets and Wakes," *Journal of Fluid Mechanics,* Vol. 88, Pt. 3, 1978, pp. 451–463.

[7]Moore, C. J., "The Role of Shear-Layer Instability Waves in Jet Exhaust Noise," *Journal of Fluid Mechanics,* Vol. 80, Pt. 2, 1977, pp. 321–367.

[8]Crow, S. C., and Champagne, F. H., "Orderly Structure in Jet Turbulence," *Journal of Fluid Mechanics,* Vol. 48, Pt. 3, 1971, pp. 547–591.

[9]Hussain, A. K. M. F., and Zaman, K. B. M. Q., "Vortex Pairing in a Circular Jet Under Controlled Excitation. Pt. 2. Coherent Structure Dynamics," *Journal of Fluid Mechanics,* Vol. 103, Pt. 3, 1981, pp. 449–491.

[10]Lepicovsky, J., Ahuja, K. K., and Burrin, R. H., "Tone Excited Jets. Pt. 3: Flow Measurement," *Journal of Sound and Vibration,* Vol. 102, No. 1, 1985, pp. 71–91.

[11]Tang, S. K., and Ko, N. W. M., "Some Behaviours of Coherent Structures Under Controlled Excitation in Coaxial Jet of Mean Velocity Ratio of 0.3," *Proceedings of IUTAM Symposium on Separated Flows and Jets* (Novosibirsk), Springer-Verlag, Berlin, 1990, pp. 879–882.

[12]Ko, N. W. M., and Tang, S. K., "Effect of External Exciter on the Far Field of an Air Jet," *Journal of Sound and Vibration,* Vol. 137, No. 1, 1990, pp. 154–158.

[13]Michalke, A., and Hermann, G., "On the Inviscid Instability of a Circular Jet with External Flow," *Journal of Fluid Mechanics,* Vol. 114, 1982, pp. 343–359.

[14]Kibens, V., "Discrete Noise Spectrum Generated by an Acoustically Excited Jet," *AIAA Journal,* Vol. 18, No. 4, 1980, pp. 434–441.

Spreading Rate of an Unsteady Turbulent Jet

H. Kouros,* R. Medina,* and H. Johari†
Worcester Polytechnic Institute, Worcester, Massachusetts 01609

Introduction

THE steady turbulent jet is a well-documented flow and has many practical applications such as ejectors and burners. A number of investigations have been carried out in which the jet flow is perturbed by harmonic oscillations of various amplitudes and frequencies.[1,2] At small forcing amplitudes and above a minimum frequency, the velocity profile spreading and volume flow rate were increased in the near field. The velocity field of fully pulsed air jets (no mass flow in between pulses) has also been studied in detail.[3] The entrainment in fully pulsed air jets was shown to be much higher than the steady or partially pulsed jets. Even though the jet spreading and volumetric entrainment were increased in these pulsatile jet flows, the basic structure of the jet did not change. The velocity profiles were self-similar; the spreading rate was linear with the downstream distance; and most importantly, the entrainment rate scaled with the square root of the aggregate jet momentum flux.[3] The results are consistent, except for the proportionality constants, with Taylor's entrainment hypothesis.[4] All of the previous pulsed jet studies seem to indicate that the steady jet characteristics are recovered once a certain downstream location is reached. In most cases only the near field is greatly altered.

Recently, Breidenthal[5] has postulated a new self-similar flow: the turbulent exponential jet. The nozzle exit velocity is required to increase exponentially in time. Breidenthal argues that the acceleration of the jet would imply a lower entrainment rate. Fang and Sill[6] measured the centerline velocities of linearly accelerating turbulent jets. The results indicate that significant deviations (lower normalized velocities) from the steady case exist in the linearly accelerating jets. These aberrations were observed even in the far field. This is interesting since the majority of pulsed jets were effective only in the near field. Unfortunately, neither the spreading rates nor the entrainment rates were reported for these monotonically changing unsteady jets.

The main purpose of this Note is to report on the penetration length and spreading rate of a nonharmonic unsteady jet of considerable duration, as compared to the pulsed jets. Flow-visualization experiments were performed on a simple apparatus. The visual measurements are closely related to the concentration field which is of prime interest in turbulent mixing problems.

Experimental Technique

The experiments were conducted in a transparent water tank having dimensions 1.2×1.2×1.5 m deep. The jet flowfield was generated by a simple apparatus which consisted of a 1.2-m-long, round clear acrylic tube held in place by a PVC plate at one end. At the other end, the tube was connected to a fluid feed line and a solenoid valve. The tube, which had a 28.6-mm inner diameter, was set vertically above the tank such that the tube exit was just below the water surface. Initially a rubber stopper was placed at the tube exit (inside the water tank) and dyed fluid was fed into the tube from a reservoir. Once the tube was filled, the solenoid valve

Received Aug. 4, 1992; revision received Feb. 15, 1993; accepted for publication Feb. 19, 1993.

*Undergraduate Student, Mechanical Engineering Department. Student Member AIAA.

†Assistant Professor, Mechanical Engineering Department. Member AIAA.

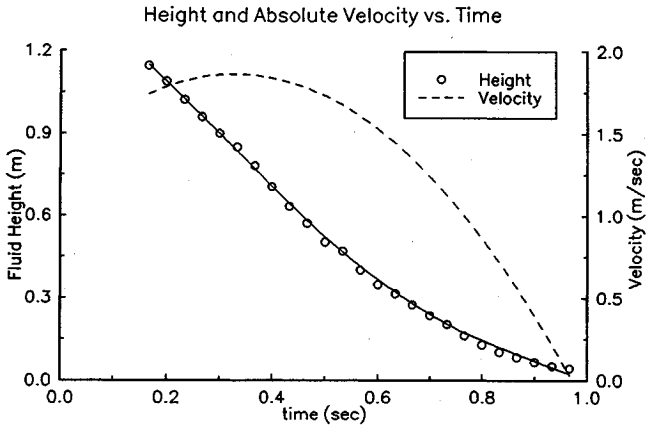

Fig. 1 Measured height and calculated velocity of the fluid inside the tube.

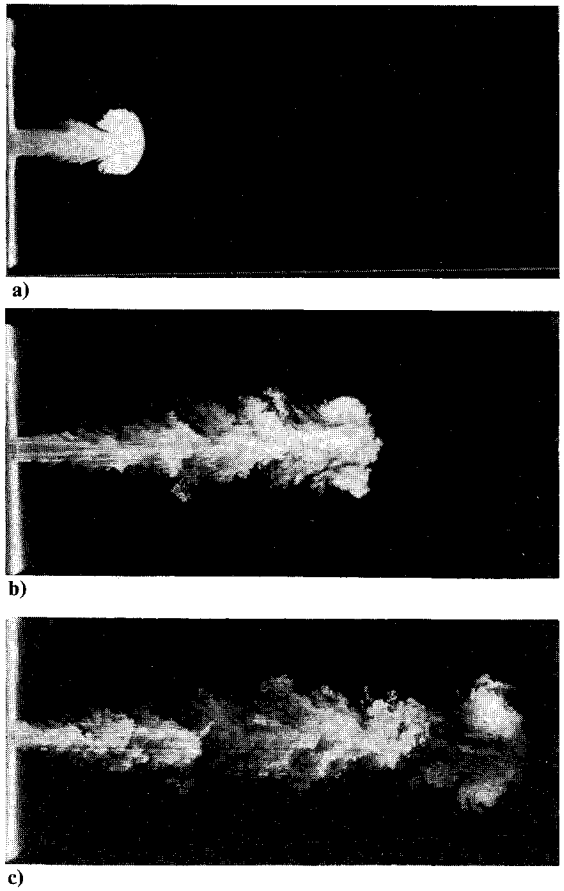

Fig. 2 LIF photographs depicting the development of the unsteady jet: a) t=0.2 s, 5d; b) t=0.5 s, 13d; and c) t=0.8 s, 18d.

was closed and the fluid was allowed to become quiescent (1–2 min). The rubber stopper was then removed carefully. A minimal amount of dye (~5 cc) diffused out of the tube prior to the start of the run. The fluid remained in place by means similar to those which keep a liquid inside a straw when one end is held airtight. Runs were started when the valve was rapidly opened. Gravity forced the dyed fluid into the water tank, thus generating an unsteady jet flow. Runs typically lasted nearly 1 s.

Both fluorescent and ordinary dyes were used for flow visualization. The combination of the fluorescent dye (disodium fluorescein) and a sheet of blue-green laser light, which propagated upward through the tank, allowed the internal structure of the jet to be observed. The typical fluorescein concentration was on the order of 10^{-7} molar. The planar images produced by the laser-induced fluorescence (LIF) technique were recorded on photographic film and videotape.

Initially a series of runs were performed in which only the tube was imaged on the video. The instantaneous fluid height in the tube was measured from three runs and then averaged to find the jet exit velocity variation in time. The averaged data were then curve fitted by a third-degree polynomial and the jet exit velocity was obtained by taking the first derivative of the polynomial. Figure 1 shows the averaged height measurements as well as the resulting velocity as a function of time. The maximum tube exit velocity was 1.86 m/s, resulting in a jet Reynolds number (based on the tube diameter) of 5.3×10^4. An important characteristic of the velocity curve is the initial acceleration of the flow up to 0.33 s and its subsequent deceleration. The density difference between the jet fluid and the tank water was kept below 0.1%. Therefore, buoyancy effects can be neglected.

Results and Discussion

The LIF photographs of a sample run in Fig. 2 (and many similar ones) illustrate the development of the unsteady jet produced by the aforementioned apparatus. Initially the jet velocity increases from zero and a starting vortex forms. The photograph in Fig. 2a depicts the jet at an elapsed time of 0.2 s and at a Reynolds number Re of 5.1×10^4. The starting vortex has traveled five jet diameters, d downstream. Based on the uniform intensity of the jet fluid (and therefore, its concentration), little mixing seems to have occurred at this stage in the evolution of the jet. A notable feature of the photograph is the relatively large and symmetric starting vortex. Evidence of early entrainment may be observed in the small incisions located at the base of the starting vortex. Figure 2b shows the intermediate stage of jet growth at an elapsed time of 0.5 s. The starting vortex has traveled 13d and the jet Re is about 4.9×10^4. Although entrainment has diluted the starting vortex, it still appears to be fairly symmetric. Large-scale lateral penetration of ambient fluid into the jet can be observed at this stage.

The jet near the end of run time appears in Fig. 2c at an elapsed time of 0.8 s. The jet Re has decreased to about 2.5×10^4. Lateral entrainment of the ambient fluid into the jet is vividly present in this photograph. The distance traveled by the starting vortex is 18d. The symmetry of the starting vortex concentration is lost here apparently due to uneven entrainment of ambient fluid. An interesting phenomenon, visible in the last photograph, is the separation of the starting vortex from the rest of the jet. This point will be further discussed.

From the data on videotape, the penetration length of the starting vortex and the visible spreading rate of the jet were recorded as a function of time. These measurements were taken at 1/12 of a second intervals and then ensemble averaged at each time instant. A total of 15 runs were used to obtain the ensemble average. The maximum uncertainty in time arises from the timing errors associated with the video recorder which is estimated to be 33 ms.

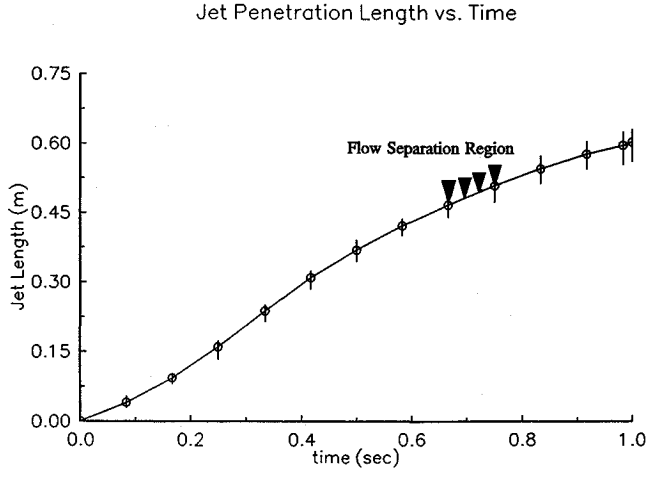

Fig. 3 Ensemble averaged penetration length of the jet starting vortex vs time. Maximum and minimum values are represented by the vertical bars.

Figure 3 shows the variation of the mean length of the jet with time. The length measurements refer to the distance traveled by the leading edge of the starting vortex. The uncertainty in measurements is approximately ±13 mm. The vertical bars on the data points indicate the maximum and minimum values of the jet penetration length at each time instant. The averaged maximum length traveled by the jet starting vortex at the end of run was 0.60 m or 21*d*.

As mentioned earlier, the starting vortex gradually separated from the rest of the jet in most of the runs. The onset of separation occurred between 16*d* and 18*d*; the starting vortex proceeded downstream faster than the tip of the turbulent jet. Although the cause of separation is unknown, a possible explanation is the rapid deceleration of the flow at the tube exit. The arrowhead symbols in Fig. 3 mark the region where splits were observed.

The most striking aspect of the present measurements is the visible spreading rate of the jet. Since the jet spreads linearly, the spreading rate was obtained by drawing lines tangent to the jet's visible edges. The estimated uncertainty in the reported values is ±10%. The averaged spreading rate ($d\delta/dx$), which ranged from 0.18 to 0.2, remained nearly constant during any run. A comparison between the spreading rate of steady jets at similar Reynolds and Mach numbers ($d\delta/dx \approx 0.44$)[7] and the present data reveals that the unsteady jet spreads at a rate which is less than half of the steady jet spreading rate. Unsteady effects seem to have caused a considerable reduction in the jet spreading rate for the first time. This is significant since all of the previous unsteady jet studies have reported increased jet spreading rates. Additionally, experimental error cannot be the source of this observation since the uncertainty is relatively small.

It is surprising that none of the previous work on unsteady jets have observed reduced spreading rates. Some speculative reasons follow. Most of the harmonic forcing is done at fairly high frequencies (10–100 Hz) implying that the flow may not have enough time to respond to successive acceleration and deceleration cycles. Even pulses which had velocity profiles similar to the present jet[3] lasted only 30 ms as compared to the 1 s of run time in our experiments. Perhaps a relatively long period of unsteadiness in the jet flow is required to alter the jet characteristics. The present findings agree with the theoretical arguments of Breidenthal[5] if the time associated with the relaxation of the jet is long in comparison with the run time. It should be kept in mind that the jet produced by our apparatus is confined to the near field during a run.

Conclusions

The visible spreading rate of an unsteady jet produced by a simple apparatus was measured to be less than half of the steady jet value. Moreover, the spreading rate remained nearly constant during the run whereas the velocity varied appreciably. These findings may play a crucial role in the understanding of unsteady effects on entrainment and mixing. Further experiments are currently underway to quantify the rate of mass diffusion in the present unsteady jet.

References

[1]Crow, S. C., and Champagne, F. H., "Orderly Structure in Jet Turbulence," *Journal of Fluid Mechanics,* Vol. 48, Pt. 3, 1971, pp. 547–591.

[2]Favre-Marinet, M., and Binder, G., "Structure des Jets Pulsants," *Journal de Mecanique,* Vol. 18, June 1979, pp. 355–394.

[3]Bremhorst, K., and Hollis, P. G., "Velocity Field of an Axisymmetric Pulsed, Subsonic Air Jet," *AIAA Journal,* Vol. 28, No. 12, 1990, pp. 2043–2049.

[4]Turner, J. S., "Turbulent Entrainment: The Development of the Entrainment Assumption and its Applications to Geophysical Flows," *Journal of Fluid Mechanics,* Vol. 173, Dec. 1986, pp. 431–471.

[5]Breidenthal, R. E., "The Turbulent Exponential Jet," *Physics of Fluids,* Vol. 29, No. 8, 1986, pp. 2346–2347.

[6]Fang, F., and Sill, B. L., "Experimental Investigation of Unsteady Submerged Axisymmetric Jets," *Journal of Hydraulic Engineering,* Vol. 113, No. 5, 1987, pp. 663–669.

[7]Dahm, W. J. A., and Dimotakis, P. E., "Measurements of Entrainment and Mixing in Turbulent Jets," *AIAA Journal,* Vol. 25, No. 9, 1987, pp. 1216–1223.

Multifluid Model of Turbulence for Li-SF_6 Submerged Combustion

S. H. Chan* and M. M. M. Abou-Ellail†
University of Wisconsin-Milwaukee, Milwaukee, Wisconsin 53201

Introduction

STORED chemical energy propulsion systems (SCEPS) using Li/SF_6 reactants have recently received considerable attention as a means of producing high energy per unit mass of reactant.[1-6] They use a liquid-metal fuel combustor as a heat source of a closed steam-power cycle. The combustor uses a liquid metal bath (alkali metal fuel) through which a high-momentum gas jet (SF_6 or other halogen gaseous oxidizer) is injected, forming a reacting multiphase submerged jet. Flame temperatures as high as 4000 K may be encountered, making detailed flame structure measurements difficult. Prior plume structure analyses[3,5] assumed phase equilibrium and local homogenous flow with equal velocity and temperature between phases and thus underpredicted the plume length. These assumptions are now removed in the present multifluid (MF) model.

Multifluid Model for Submerged Combustion

The Li-SF_6 reacting flow patterns[6] are somewhat similar to the conventional two-phase flow,[7] in which the void fraction can range between zero and one, flow regimes can change, and the interaction between the two phases is strong. However, it is necessarily extended to reacting multiphase flow to account for not only reaction and velocity slip between phases but also phase nonequilibrium.

The proposed physical model treats the composition of the multiphase submerged flame as a number of "fluids" or phases. The total number of fluids is *n;* any flow or thermochemical property ϕ pertaining to fluid k ($1 \le k \le n$) is designated by a k superscript, e.g., ϕ^k. The last two fluids (fluid $n-1$ and fluid n) are, respectively, the dispersed condensed combustion products [such as LiF(ℓ), Li_2S(ℓ) and LiF(s)] and the continuous gas phase [such as SF_6(g), Li(g), Li_2F_2(g), Li_3F_3(g), and Li_2S(g), etc.]. The remaining fluids ($1 \le k < n-2$) are the dispersed Li droplet phases; each fluid is characterized by a mean droplet diameter D^k, with the smallest diameter at $k = 1$. The mass conservation equation for fluid k is

$$[\bar{\rho}^k \bar{\alpha}^k \bar{u}_i^k - (\mu_t^k/\sigma_\alpha^k)\bar{\alpha}_{,i}^k]_{,i} = \dot{S}_m'^k \tag{1}$$

where the comma suffix denotes differentiation with respect to the spatial coordinates; μ_t^k, σ_α^k, and $\bar{\alpha}^k$ are, respectively, the turbulent viscosity, turbulent Schmidt number, and the mean volume fraction of fluid k; $\bar{u}_i^k$ is the mean velocity in the i direction; $\bar{\rho}^k$ is the density; and $\dot{S}_m'^k$ is a volumetric mass source term due to evaporation, condensation, and droplet interfluid transfer as droplets decrease in size given by

$$\dot{S}_m'^k = \dot{m}'^{k+1}\bar{\alpha}^{k+1} - (\dot{m}'^k + \dot{m}_v'^k)\bar{\alpha}^k \qquad 1 \le k \le n-2 \tag{2}$$

$$\dot{S}_m'^k = \sum_{\ell=1}^{n-1} \dot{m}_v'^\ell \bar{\alpha}^\ell - \dot{m}'^k \bar{\alpha}^k \qquad k = n \tag{3}$$

Received May 11, 1992; presented as Paper 92-3137 at the AIAA/SAE/ASME/ASEE 28th Joint Propulsion Conference, Nashville, TN, July 6–8, 1992; revision received Oct. 20, 1992; accepted for publication Oct. 20, 1992.

*Wisconsin Distinguished Professor, Department of Mechanical Engineering.

†Visiting Professor, Department of Mechanical Engineering; currently, Professor, Department of Mechanical Engineering, Cairo University, Cairo, Egypt.